Cohesive Acceleration and Focusing of Relativistic Electrons in Overdense Plasma

V. Yakimenko,[1] I.V. Pogorelsky,[1] I.V. Pavlishin,[1] I. Ben-Zvi,[1] K. Kusche,[1] Yu. Eidelman,[1] T. Hirose,[2] T. Kumita,[3] Y. Kamiya,[3] J. Urakawa,[4] B. Greenberg,[5] and A. Zigler[5]

[1]*Accelerator Test Facility, Brookhaven National Laboratory, 820, Upton, New York 11973, USA*
[2]*Advanced Research Institute for Science and Engineering, Waseda University, Shinjuku-ku, Tokyo 169-8555, Japan*
[3]*Department of Physics, Tokyo Metropolitan University, Hachioji-shi, Tokyo 192-0397, Japan*
[4]*KEK (High Energy Accelerator Research Organization, Tsukuba-shi, Ibaraki 305-0801, Japan*
[5]*Racah Institute of Physics, The Hebrew University, 91904 Jerusalem, Israel*

(Received 2 January 2003; published 3 July 2003)

We describe our studies of the generation of plasma wake fields by a relativistic electron bunch and of phasing between the longitudinal and transverse fields in the wake. The leading edge of the electron bunch excites a high-amplitude plasma wake inside the overdense plasma column, and the acceleration and focusing wake fields are probed by the bunch tail. By monitoring the dependence of the acceleration upon the plasma's density, we approached the beam-matching condition and achieved an energy gain of 0.6 MeV over the 17 mm plasma length, corresponding to an average acceleration gradient of 35 MeV/m. Wake-induced modulation in energy and angular divergence of the electron bunch are mapped within a wide range of plasma density. We confirm a theoretical prediction about the phase offset between the accelerating and focusing components of plasma wake.

DOI: 10.1103/PhysRevLett.91.014802 PACS numbers: 41.75.Lx, 41.75.Ht, 52.35.–g

Plasma-based accelerator schemes use laser (LWFAs) or electron beams (PWFAs) to drive plasma waves that induce ultrahigh acceleration gradients not achievable with conventional radio-frequency accelerators. The PWFA mechanism [1] uses a highly relativistic electron beam propagating in plasma to excite a large amplitude wake field that can accelerate a second trailing electron bunch to high energy. Recognizing that precise control of the transverse dynamics of an accelerating beam is crucial for reaching the necessary high luminosity in an accelerator, features of the motion of transverse particles have attracted considerable interest.

A fundamental feature of wake field acceleration is the phase offset between the longitudinal and radial forces in the wake. This statement follows from the Panofski-Wenzel theorem [2] that relates these forces by the equation

$$\frac{\partial E_z}{\partial r} = \frac{\partial (E_r - B_\theta)}{\partial \xi}, \tag{1}$$

where $\xi = (k_p z - \omega_p t)$. For a linear regime, these forces take a simple analytical form

$$E_z \propto \cos\xi, \qquad E_r - B_\theta \propto r \sin\xi, \tag{2}$$

implying that there is a $p/2$ phase offset between the longitudinal and radial fields. Thus, attaining stable acceleration in the plasma's wake field requires precisely placing the accelerated particles in the relatively narrow window within the wake, where both acceleration and focusing are maintained simultaneously.

In Experiment E157 at SLAC, a change in plasma focusing was observed along the bunch, using an externally imposed energy chirp [3,4]. Yet, although this finding was fundamentally important, the phasing between the accelerating and focusing components in the wake field lacked empirical verification. Our study provides the first observation of such phase correlation in the linear overdense regime, $n_e \gg n_b$. This regime fosters a simplified analytical treatment, yet still offers the maximum accelerating fields for technically achievable bunch charges, provided that the resonance condition between the plasma and electron bunch is attained. We will show that our experiment met this condition.

The PWFA experiment, set in beam line 1 of the Brookhaven Accelerator Test Facility, used as a plasma source a 60-MeV electron beam produced by a photocathode rf electron gun followed by rf linac and a capillary electrical discharge. The plasma source is described in detail elsewhere [5]. The polypropylene capillary was 17 mm long with an inner diameter of 1 mm. It was mounted on a combination of translation and tilt manipulators to align the capillary along the path of the electron beam. The electron density of the highly ionized carbon-hydrogen plasma, produced by applying a 20-kV voltage pulse to the capillary's electrodes, reached $n_e \sim 5 \times 10^{17}$ cm^{-3}. Off-line optical interferometry [6], MHD simulations, and measurements of the CO_2 laser-energy absorption confirmed this number. Lower density levels can be obtained easily in the afterglow plasma after terminating the discharge.

The $E_e = 60$ MeV, 300 pC, 1.5 ps (rms) long electron beam was focused to an rms spot size of $\sigma_r \sim 100$ μm in the capillary discharge by upstream quadrupole triplet magnets. Because of ballistic compression in the linac, the electron beam is not Gaussian in time. It has a

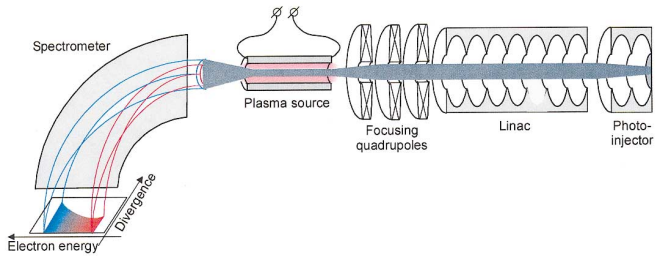

FIG. 1 (color). Schematic diagram of the plasma and electron beam interaction experiment.

fast-rising leading edge with an rms size of about $\sigma_z = 0.5$ ps that carries a charge of approximately $Q \gg 100$ pC; this is followed by a tail of ~1.5 ps (rms) [7].

The electron beam's parameters, alignment, and timing with respect to the capillary discharge were observed with electron-beam profile monitors (BPM) located before and after the plasma source, a strip-line monitor, and a Faraday cup. The primary diagnostic used was a high-resolution electron spectrometer located after the interaction cell, composed of a quadrupole magnet, a 90° dipole, and a phosphor BPM. The spectrometer chromatically focuses the beamlets in the bend plane, and maps the angular distribution of electrons on the perpendicular axis. Figure 1 is a schema of the experiment and illustrates this feature of the spectrometer.

We recorded a sequence of spectrometer images at variable time delays after the electrical discharge that generates the plasma. The spectrometer shows that the electron beam passing the plasma column acquires energy modulation, caused by the plasma wake driven by the leading head of the bunch. The amplitude of the acquired electron-energy spread evolves with the time delay, passing a maximum at $\Delta t = 2$ μs, as shown in Fig. 2. At this time, the decaying plasma density achieves resonance with the head of the electron bunch, maximizing the wake's amplitude.

In addition to the spectrometer measurements, we took beam-profile images in the straight-ahead screen with the magnets turned off. They show a uniform radial divergence (not illustrated in this paper). Thus, we confirm that the spectrometer's energy axis is dominated by the change in energy, and not by divergence or hose instability.

The resonance dependence of the wake's amplitude upon the parameter $k_p\sigma_z$, where $k_p = \frac{2e}{c}\sqrt{\frac{\pi n_e}{m_e}}$ is the plasma wave number, is described by the formula [8]

$$E_z \propto (k_p\sigma_z)^2 \exp[-(k_p\sigma_z)^2/4]. \quad (3)$$

Equation (3) reaches a maximum at the resonance condition $k_p\sigma_z \sim \sqrt{2}$ that, for $\sigma_z = 0.5$ ps, corresponds to the plasma density $n_e \sim 3.6 \times 10^{16}$ cm^{-3}. Applying Eq. (3) to the experimental curve on Fig. 2 gives us the time evolution of the average plasma density in the

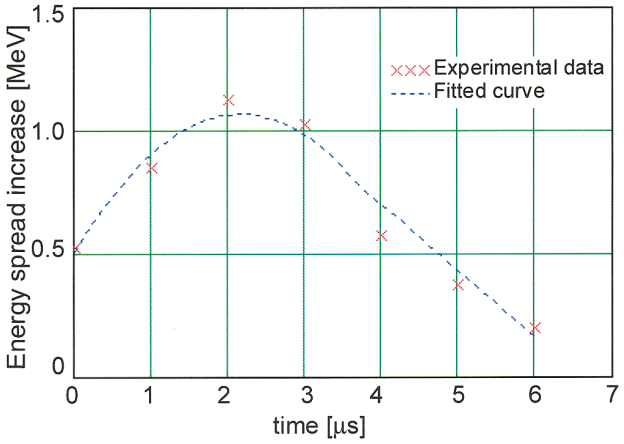

FIG. 2 (color). The measured electron energy spread as a function of time delay after the termination of the discharge.

plasma column. A zero time delay corresponds to 500 ns after triggering the discharge that lasts about 300 ns. Our measurements are taken when there is no discharge current. We see then that the exponential curve shown in Fig. 3 approximates well to the points obtained by translating the experimental data from Fig. 2 using Eq. (3). The prime cause for the exponential decay of the plasma is its hydrodynamic expansion through the capillary openings [9]. Systematic deviation of the experimental points from the exponential curve at small time delays, $\Delta t < 2$ μs, can be similarly explained by plasma depletion near these openings. We can expect that during the decay of the plasma, the matching condition is first met at the peripheral regions of the capillary. Later, the plasma density reaches the resonance in the central region of the capillary, but drops below it at the ends. Evidently, this process smooths the net energy gain as compared to Eq. (3), and adds to the validity of the exponential density dependence over the whole delay range.

The measured maximum acceleration $\Delta E_e = 0.6$ MeV that we achieved in our experiment is equivalent to a gradient of ~35 MeV/m over the 17-mm plasma length,

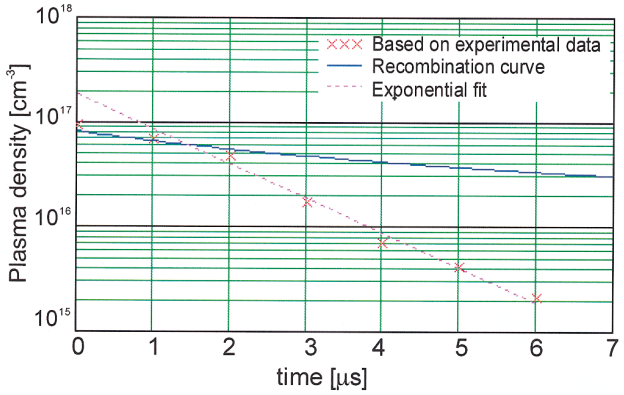

FIG. 3 (color). Calculated plasma density as a function of time delay after the termination of the discharge.

assuming that the wake field is uniform along the plasma channel. In fact, due to the longitudinal nonuniformity of the plasma density, discussed above, the actual peak acceleration gradient is even higher.

The maximum acceleration gradient in the overdense regime $n_e \gg n_b$, where $n_b \approx 10^{15}$ cm^{-3} is the average electron density in the bunch, can be estimated by the formula [10,11]

$$eE_z^{\max} \approx 150[\mathrm{MeV/m}]Q[\mathrm{nC}]/\sigma_z^2[\mathrm{ps}]. \quad (4)$$

Substituting the driver parameters into Eq. (4), we obtain $eE_z^{\max} = 60$ MeV/m, a value that is in the right range to compare with the experimentally measured number.

Figure 4 illustrates typical patterns of the electron beams observed on the spectrometer's screen. The energy distribution in the beam is shown along the horizontal axis. The transverse size of the beam on the screen is defined by the electron beam's angular divergence at the exit of the capillary.

Figure 4(a) demonstrates the initial energy and angular distribution in the beam passing the capillary without a plasma discharge. Its horizontal width is a combination of the intrinsic energy spread and the spectrometer's resolution. The transverse shape defined by the electron beam's angular divergence after the focal point of the quadrupole lens is at least an order of magnitude above the natural divergence of the electron beam due to intrinsic emittance.

A sample image Fig. 4(b), obtained at $\Delta t = 3$ μs, illustrates the typical energy modulation and focusing/defocusing effects produced by the beam's interaction with the plasma. We see that the distribution of the electron bunch exhibits strong energy modulation with two distinctive maxima, in the accelerated and decelerated portions of the electron ensemble. We notice also significant focusing and defocusing effects in the beam that are energy dependent.

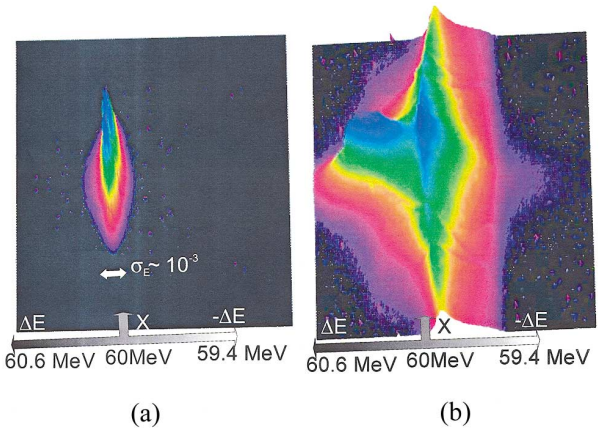

(a) (b)

FIG. 4 (color). Spectrometer images, showing intensity in a combined false-color and contour plot. Energy is shown on the horizontal axis and transverse size in the vertical axis: (a) plasma off, (b) plasma on, $\Delta t = 3$ μs.

The "double-hump" feature in the spectrum is characteristic of the sinusoidal-like modulation of electron energy in the plasma wave where a relatively high proportion of the electron population is concentrated at the maximum and minimum of the sinusoidal curve. This is the first time that such highly visible double humps have been obtained in a PWFA experiment; they indicate the uniformity of the wake field within the electron bunch.

The maximum angle of the dynamic focusing/defocusing of the electron beam in the plasma is 10 mrad, as measured on the spectrometer screen. This number agrees with a simple estimate

$$\alpha = \frac{\Delta E_e}{E_e}\frac{2}{k_p\sigma_r} \quad (5)$$

based on calculation of the radial momentum being proportional to the longitudinal acceleration ΔE_e.

We analyze Fig. 4 by studying the transverse distribution of small intervals in the energy coordinate, referring to them as slices in energy. For the sake of clarity of presentation, the energy slices are denoted with a phase Ψ, assuming a sinusoidal energy modulation with a maximum acceleration at $\Psi = 90°$. The analysis of longitudinally sliced transverse distributions reveals an interesting tendency. The transverse profile of an energy interval (slice) taken close to the maximum- and minimum-energy extremes can be approximated well by a single Gaussian curve compatible in width to the initial (no plasma) image [see Fig. 5(a)]. Distributions taken from intermediate energy slices fit into the double-Gaussian approximation. For example, the slice at $\Psi = -45°$ [see Fig. 5(b)] contains two overlapping, focused and defocused Gaussian distributions, with relative amplitudes 2:1 and $\sigma_F = 0.8$ mm, $\sigma_D = 2$ mm, correspondingly.

This initially puzzling double-Gaussian structure becomes understandable by applying a simple graphic illustration in Fig. 6 that shows the longitudinal and radial fields as $\sin(\omega_p t)$ and $\cos(\omega_p t)$ plots [see Eq. (2)].

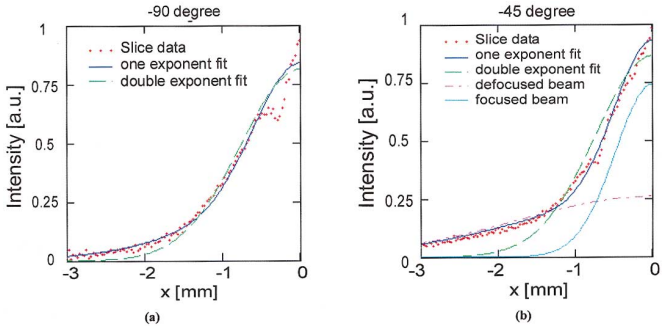

FIG. 5 (color). Sample energy slices from the spectrometer image Fig. 4(a) showing the best Gaussian fitting.

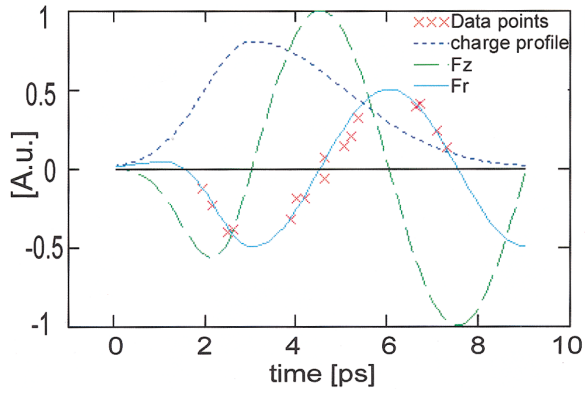

FIG. 6 (color). Expected phasing of longitudinal and transverse wake forces induced by the bunch, and experimental points reconstructed from the energy slices using double-Gaussian fit.

Evidently, the radial field crosses the zero axis at phases that correspond to a maximum or minimum of the longitudinal field. This confirms the first observation that the maximum and minimum energy slices closely reproduce the initial single Gaussian distribution obtained on the spectrometer without plasma. At any intermediate amplitude of the longitudinal field, we can identify two phases of the radial field where the polarity is different. This explains the observation of focused and defocused beamlets for each energy slice (double-Gaussian distributions) combined at different amplitudes due to the beam's time-varying density.

The experimental data points in Fig. 6 are reconstructed from the double-Gaussian approximations applied to the sliced energy distributions. Estimating the magnitude of focusing and defocusing for each energy slice, we can account for the known dynamic modulation of the electron emittance over the bunch length [12], and the variation in the density of the plasma electrons along the bunch [3] unrelated to the focusing induced by the wake's accelerating field. We eliminate this trend in the input beam's divergence by calculating a floating initial divergence $\overline{\sigma} = (\sigma_F + \sigma_D)/2$ for each energy slice. This assumes there is symmetrical focusing and defocusing around the initial divergence. Undoubtedly, such analysis may be affected by beam loading that distorts and depletes the wake's amplitude and by the fact that σ_F and σ_D represent different slices spaced in time (up to 1/3 of the plasma period in our measurements). Still, the normalized data points $\pm(\sigma_D - \overline{\sigma})/\overline{\sigma}$ on Fig. 6 fit surprisingly well into the expected sinusoidal variation confirming our initial assumption about the $\pi/2$ phase shift between the longitudinal and radial components of the wake field.

To summarize, our study shows that the electron focusing in the plasma wake field is amplitude correlated to the accelerating field. Furthermore, it provides evidence that the phase offset between the longitudinal and transverse components of the wake field is $\pi/2$, the same as in conventional rf accelerators. The conclusion is that accelerators of the plasma wake field would allow a certain phase range to provide both for accelerating and transverse focusing of the particle beams.

Future plans include using the microbunched beam at a 10.6 μm period to enhance excitation of the wake by the electron beam, and to improve plasma diagnostics including the interferometer technique.

The authors thank M. Zolotorev for helpful discussions. This study is supported by the U.S. Department of Energy under the Contract No. DE-AC02-76CH00016 and Japan-U.S. and Japan-Israel Cooperative Grants in High Energy Physics.

[1] P. Chen, J. M. Dawson, R.W. Huff, and T. Katsouleas, Phys. Rev. Lett. **54**, 693 (1985).
[2] R. D. Ruth *et al.*, Part. Accel. **17**, 171 (1985).
[3] C. O'Connell *et al.*, Phys. Rev. ST Accel. Beam **5**, 121301 (2002).
[4] M. J. Hogan *et al.*, in *Advanced Accelerator Concepts*, Proceedings of the Tenth Workshop, AIP Conf. Proc. No. 647 (AIP, New York, 2002), p. 3.
[5] D. Kaganovich, P.V. Sasorov, Y. Ehrlich, C. Cohen, and Z. Zigler, Appl. Phys. Lett. **71**, 2925 (1997).
[6] D. Kaganovich, P. Sasorov, C. Cohen, and Z. Zigler, Appl. Phys. Lett. **75**, 772 (1999).
[7] P. Catravas *et al.*, Phys. Rev. Lett. **82**, 5261 (1999).
[8] P. Sprangle, E. Esarey, A. Ting, and G. Joyce, Appl. Phys. Lett. **53**, 2146 (1988).
[9] N. A. Bobrova *et al.*, Phys. Rev. E **65**, 016407 (2002).
[10] S. Lee *et al.*, Phys. Rev. E **61**, 7014 (2000).
[11] E. Esarey *et al.*, IEEE Trans. Plasma Sci. **24**, 252 (1996).
[12] X. Qiu, K. Batchelor, I. Ben-Zvi, and X-J. Wang, Phys. Rev. Lett. **76**, 3723 (1996).